

## LITHOSPHERIC STRUCTURE IN THE PACIFIC GEOID

B.D. Marsh and J.H. Hinojosa  
Dept. of Earth and Planetary Sciences  
The Johns Hopkins University  
Baltimore, Maryland 21218

The high degree and order ( $n, m > 12, 12$ ) SEASAT geoid in the central Pacific correlates closely with the structure of the cooling lithosphere. Relative changes in plate age across major fracture zones in relatively young ( $\leq 80$  Ma) seafloor frame the east-west trending pattern formed by the geoid anomalies (Figure 1). The separation of the major fracture zones is  $\sim 1000$  km, whereas the dominant wavelength of the geoid field is  $\sim 2000$  km in the north-south direction.

Investigators customarily remove the effects of regional lithospheric thermal subsidence from bathymetry to expose anomalies in depth. This field removal in bathymetry corresponds to removal of some of the low degree and order ( $n, m \leq 12, 12$ ) geoidal components, and the step-like structure across fracture zones is also removed. We have, instead, removed the regional thermal subsidence from the bathymetry by subtracting a mean subsidence surface from the observed bathymetry. This produces a residual bathymetry map (Figure 2) analogous to the usual residual depth anomaly maps. The residual bathymetry obtained in this way then contains shallow depths for young seafloor, and larger depths for older seafloor, thus retaining the structure of the lithosphere while removing the subsidence of the lithosphere.

In order that sub-lithospheric density variations be revealed with the geoid, the regional geoid anomalies ( $\sim 2$  m) associated with bathymetric variations, must first be removed. We have used spectral techniques to generate a synthetic geoid (Figure 3) by filtering the residual bathymetry assuming an Airy-type isostatic compensation model. We have assumed a value of 100 km for the thickness of the lithosphere, and have also assumed the plane approximation to be valid. The resulting field fairly closely resembles in pattern the observed geoid of Figure 1, but the amplitudes are different, and may yet need to be adjusted through the depth of compensation and density structure. It is, nevertheless, clear that this field due to lithospheric structure may be a major component of the geoid in this region.

A comparison of the observed admittance with model admittances shows that, for the region under study, no single compensation mechanism will explain all of the power in the geoid. Our values of the admittance for the shorter wavelengths ( $\lambda \leq 450$  km) agree with the values obtained by Sandwell & Poehls (1980) for a similar region in the Pacific assuming an Airy model. The longer wavelengths do not agree with the Airy model, nor do they agree with the thermal compensation

model. This may most likely be due to the fact that the spectral contributions from the Hawaiian swell and from the regional Pacific bathymetry are indistinguishable in the frequency domain. Nevertheless, because topographic features are mainly coherent with the geoid, to first order an isostatically compensated lithosphere cut by major E-W fracture zones accounts for most of the power in the high degree and order SEASAT geoid in the central Pacific.

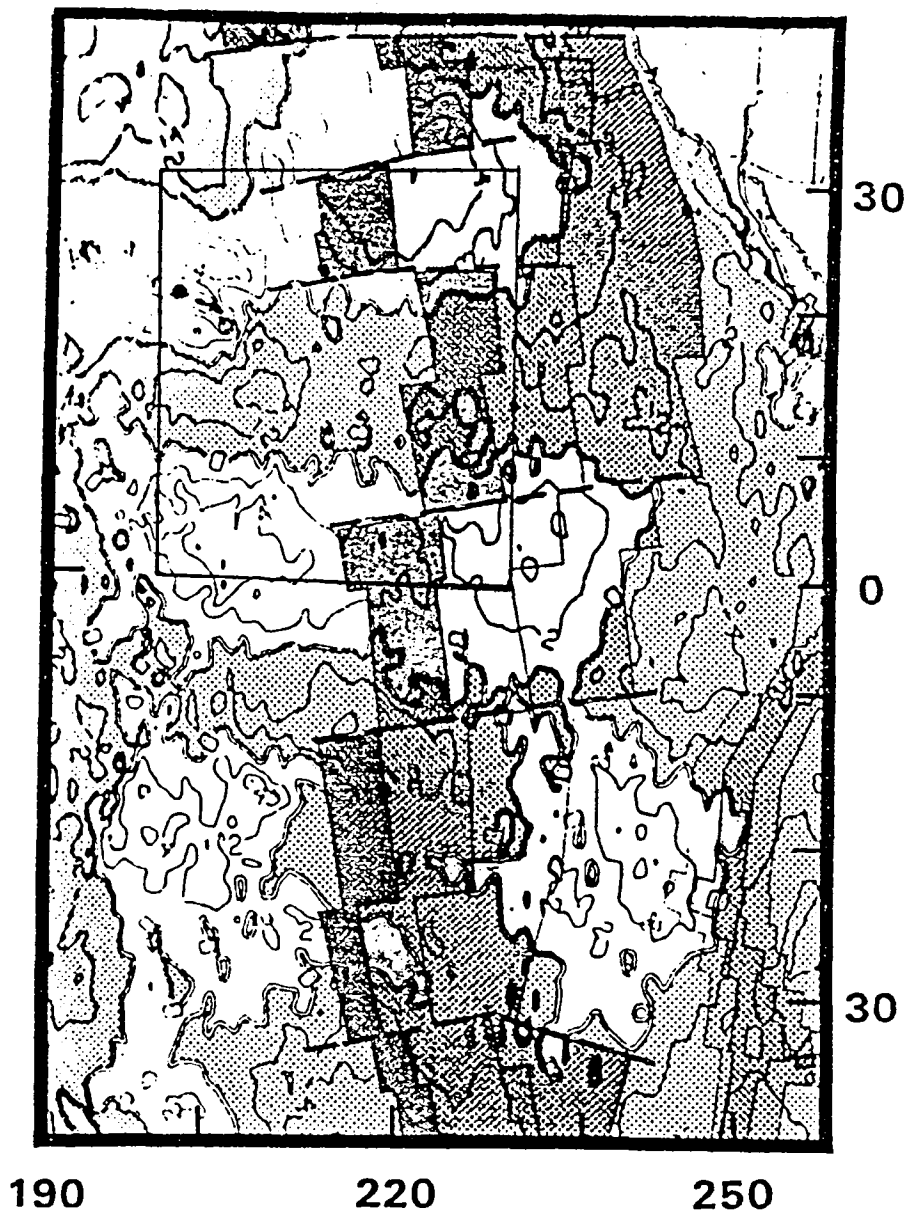


Figure 1. The SEASAT geoid superimposed on the map of the age of the ocean basins of Pitman et al. (1974). Major fracture zones with large offsets have been marked with dashed lines. From north to south, these fracture zones are Mendocino, Murray, Molokai, Clipperton, and Marquesas and the last is apparently unnamed. These fracture zones frame the pattern of geoid anomalies, and there is a correlation between regions of relatively young seafloor and positive geoid anomalies.

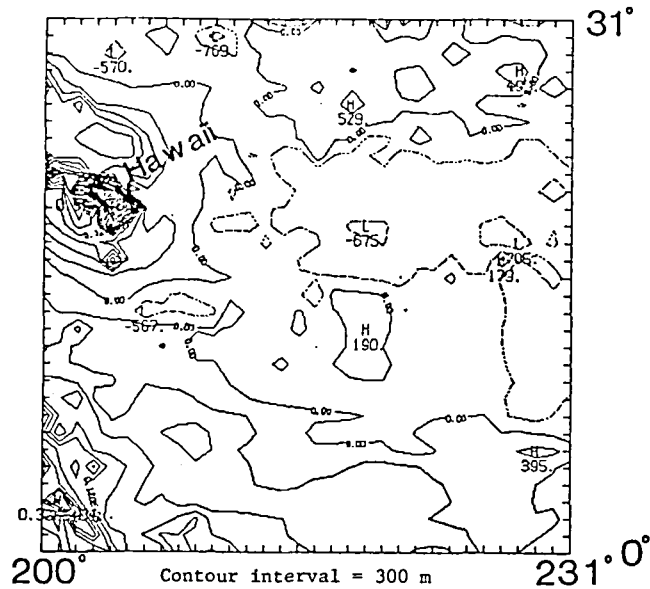


Figure 2. The residual bathymetry obtained by removing a mean thermal subsidence surface from the observed bathymetry. Large positive values occur over shallow, young seafloor, and large negative values over deep, older seafloor.

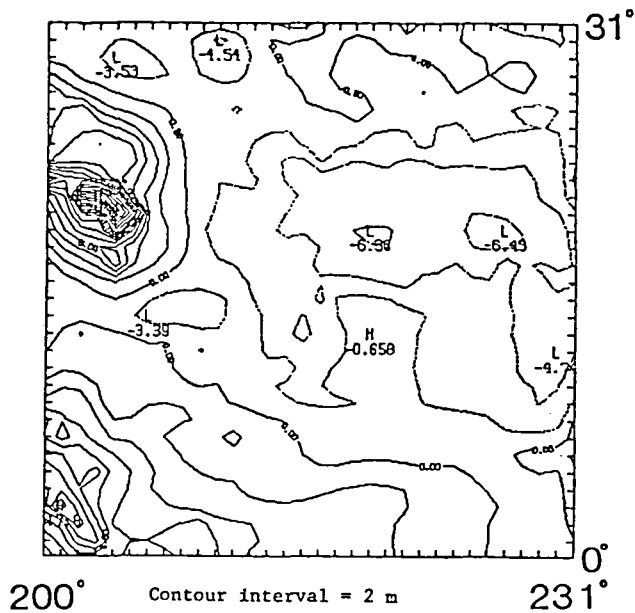


Figure 3. The synthetic geoid obtained by filtering the residual bathymetry in Figure 2 through an Airy-type isostatic compensation model.